NANO LETTERS

2005
Vol. 5, No. 2
235−241

# Electrical Docking of Microtubules for Kinesin-Driven Motility in Nanostructures

**Martin G. L. van den Heuvel,[†] Christopher T. Butcher,[†] Serge G. Lemay,[†] Stefan Diez,[‡] and Cees Dekker*,[†]**

*Kavli Institute of Nanoscience, Section Molecular Biophysics, Delft University of Technology, Lorentweg 1, 2628 CJ Delft, The Netherlands and Max Planck Institute of Molecular Cell Biology and Genetics, Pfotenhauerstrasse 108, 01307 Dresden, Germany*

*Received October 18, 2004; Revised Manuscript Received December 15, 2004*

**ABSTRACT**

**We demonstrate localized electrical control of the docking of microtubules onto engineered kinesin-coated structures. After applying a voltage to a gold electrode, we observe an enhanced transport of microtubules from solution toward the surface and a subsequent increase of the amount of moving microtubule shuttles. Switching off the voltage leads to a partial detachment of microtubules from the surface. The surface coverage of microtubules, during both the docking and undocking events, follows an exponential time dependence. We provide a simple kinetic model, incorporating the equilibrium between free and surface-bound microtubules, that explains these data.**

The biological cell possesses a variety of force generating elements to perform mechanical work. For example, kinesin motor proteins can bind some cargo and walk along microtubules, their associated protein filaments, thus providing a means of directed intracellular transport of material. Another well-known example of force generation is the contracting muscle system, caused by myosin motors that translocate actin filaments. Both kinesin and myosin derive energy from the hydrolysis of adenosine trisphosphate (ATP). Exploitation of biomolecular motors in a nanofabricated environment will open up ways of controlling matter on the nanoscale,[1,2] for example the transport of DNA molecules[3] or polystyrene beads.[4] Recent work has concentrated on using the filaments as transporting shuttles[3−5] that glide over motor-protein-coated surfaces. Micro- and nanofabrication techniques, chemical patterning, and combinations thereof have been used to create well-defined tracks for filament shuttles (microtubules[4,6−9] or actin[10−12]), allowing spatial control over the motility. Electric fields that can be switched on and off in time have been used to influence velocity and orientation of microtubules[6,13] and actin filaments[14,15] in motility assays at a large (∼mm) macroscopic scale. Combined spatial and temporal control over microtubule motility has, however, not been reported until now.

In this paper we report the use of localized electric fields to control the transport of negatively charged microtubule shuttles from bulk solution into nanoengineered structures on a substrate. When scaling down the tracks for microtubule motility toward smaller dimensions, there is a need for a more efficient docking of microtubules into those structures. One way to achieve this would be to use large kinesin-coated areas that collect microtubules from solution and feed them into the network of tracks (Figure 1a). The use of nanofabrication techniques allows for an easy coupling between the microscopic docking pads and the nanosized microtubule tracks. Another tool, which does allow additional control, is to use switchable electric fields to drive microtubules toward the substrate. Nanofabrication makes it possible to integrate the electrodes into the structures, thereby enabling the control of shuttle docking at specific places on a substrate.

To demonstrate the electrical docking of microtubules, we used nanofabrication techniques to fabricate gold (Au) electrodes in recessed areas in silicon dioxide ($SiO_2$) substrates (Figure 1a) and chemical patterning to block motility on the $SiO_2$. The details of the fabrication process involve the following. Onto a silicon (Si) substrate with a 1 $\mu$m thick layer of thermally grown $SiO_2$, an electron-beam (e-beam) sensitive resist layer of 600 nm was spun. The patterns were defined by e-beam lithography, and a reactive ion-etching step then transferred the pattern into the $SiO_2$. Finally, e-beam evaporation was used to deposit a 5 nm thick chromium (Cr) sticking layer and a 30 nm thick Au layer.

* Corresponding author. Fax: +31-15-2781202; E-mail: dekker@mb.tn.tudelft.nl.
[†] Delft University of Technology.
[‡] Max Planck Institute of Molecular Cell Biology and Genetics.

10.1021/nl048291n CCC: $30.25 
**Published on Web 01/08/2005**

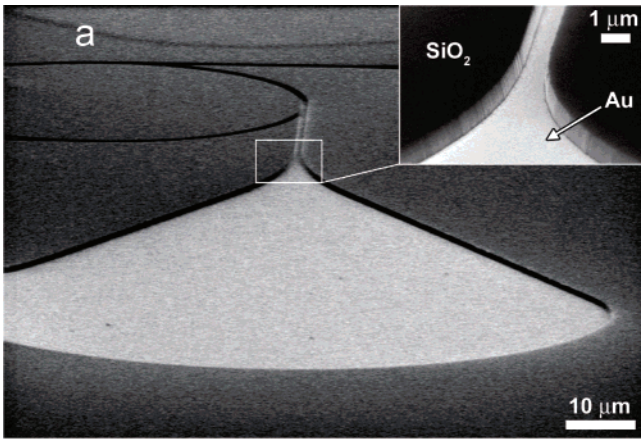


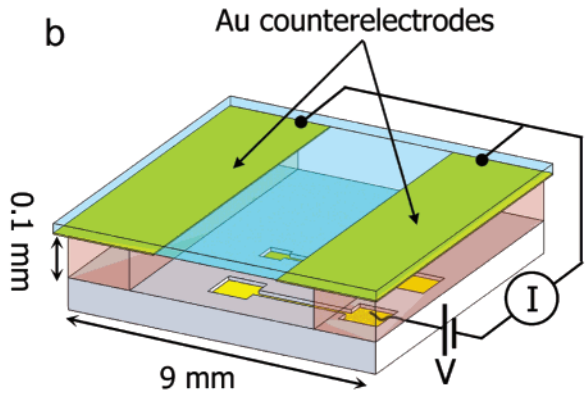


**Figure 1.** (a) Scanning electron microscope (SEM) image of a nanofabricated structure serving as a track for microtubule motility. The large droplet-shaped area is a docking place for microtubule shuttles from solution. The inset shows the connection of the docking area into the circular structure. The tracks consist of recessed areas in the $SiO_2$ substrates (see inset, depth ~860 nm), with a gold-covered bottom. (b) Schematic layout of a flow cell (not to scale). Square test microstructures (yellow) are fabricated in the substrate, according to the process described in the text. Similar to the SEM pictures in (a), the structures consist of gold areas recessed into $SiO_2$. They are connected to bonding pads at the edge of the chip via small leads. Two 0.1 mm thick spacers cover the bonding pads and part of the connection leads. The top of the flow cell consists of a cover slide with an Au counter electrode at the inside. A transparent window is kept open for microscopy imaging. Voltages ($V$) were applied between the test structures and the counter electrode and the resulting current ($I$) was measured.

This was followed by a lift-off step to remove the resist. The samples were subsequently cleaned and a hydrophilic poly-ethylene-glycol (PEG) ([methoxy(poly-ethyleneoxy)-propyl]-trimethoxysilane, 90%, ABCR Karlsruhe) self-assembled monolayer (SAM) was grafted onto the $SiO_2$. Finally, a hydrophobic hexadecanethiol-SAM was grafted onto the gold. In the experiments, we used 9 × 9 $mm^2$ substrates on which square test structures with lengths of 50 and 100 $\mu$m were fabricated. Two small leads (2000 × 2 $\mu m^2$) connected the test structures to bonding electrodes at the edge of the substrate. The bonding electrodes were connected to the outside electronics by wire bonding. A flow cell (Figure 1b) was built by putting two spacers (~0.1 mm thick Parafilm or Scotch double-sided tape) over the bonding electrodes and part of the leads and covering the chip with a microscope slide (24 × 24 $mm^2$). A 0.1 $\mu$m thick gold layer was evaporated on the cover slide as the counter electrode. A transparent window of width ~3 mm was kept free from gold to allow for imaging.

Microtubule motility was imaged by fluorescence microscopy with an inverted Olympus microscope (Zeiss 100× oil-objective, 1.30 NA) and images were recorded with a CCD camera (Hamamatsu ORCA). The flow cell was first incubated for 5 min with a casein solution (0.5 mg/mL casein in BRB80 buffer (80 mM pipes, 1 mM $MgCl_2$, 1 mM EGTA, pH = 6.9)) to passivate the Au surface. Then a kinesin-containing solution was perfused into the flow cell (6 $\mu$g/mL full-length *Drosophila* conventional kinesin in BRB80, 0.2 mg/mL casein, 1 mM ATP) and incubated for 5 min. Finally, the flow cell contents were exchanged with motility solution containing rhodamine-labeled paclitaxel-stabilized microtubules[16] (~30 nM tubulin, 1 mM ATP, 1 mM $MgCl_2$, 10 $\mu$M Taxol), an anti-bleaching cocktail (20 mM D-glucose, 0.020 mg/mL glucose oxidase, 0.008 mg/mL catalase, 1% $\beta$-mercaptoethanol ($\beta$ME)), and a redox mediator (3 mM ferrocene-dimethanol ($Fc(MeOH)_2$)), all in BRB80 buffer. As intended, microtubules could be visualized moving on both the cover slide as well as on the gold, but not on the $SiO_2$. Voltage pulses were applied to the microelectrode, with a duration of 30 to 90 s and with amplitudes between +0.5 and +1.2 V (with respect to the counter electrode). Fluorescence images were taken each second. For both the application of the voltages and the monitoring of the resulting current, an electrochemical potentiostat (BAS CV50W) was used in a two-electrode setup.

Figure 2 shows the increasing density of microtubules upon applying a voltage to an electrode. A typical sequence of snapshots from a movie is displayed, as taken during and after the application of a voltage. Initially (Figure 2a), the number of microtubules present at the gold surface inside the square structure is limited. Then, at $t = 0$ s, a voltage of 0.7 V is applied during 60 s and the number of microtubules at the electrode surface starts to increase with time ($t = 20$ s, $t = 60$ s). After switching off the voltage, (at $t = 60$ s), the number of microtubules that are moving on the gold surface gradually decreases again. Microtubules were seen to detach from the gold either by spontaneous release or by collisions with the $SiO_2$ walls of the structure. At $t = 120$ s (60 s after switching off the voltage), the number of microtubules inside the structure has decreased considerably, although there are still more than at the beginning of the docking event (cf. Figure 2a, $t = 0$ vs $t = 120$ s). In general, motility was observed to continue unimpeded during bias, although some microtubules got stuck to the gold after landing. In some rare cases, motility was slowed or halted during application of the voltage. Motility on the $SiO_2$ substrate (i.e., outside the square area in Figure 2) was not observed due to the blocking by the PEG monolayer.

To analyze the docking efficiency of microtubules, we quantify the amount of microtubules present in each camera image. In an automated fashion we count the total number of pixels belonging to microtubule particles in each frame. The latter number serves to quantify the microtubule density.

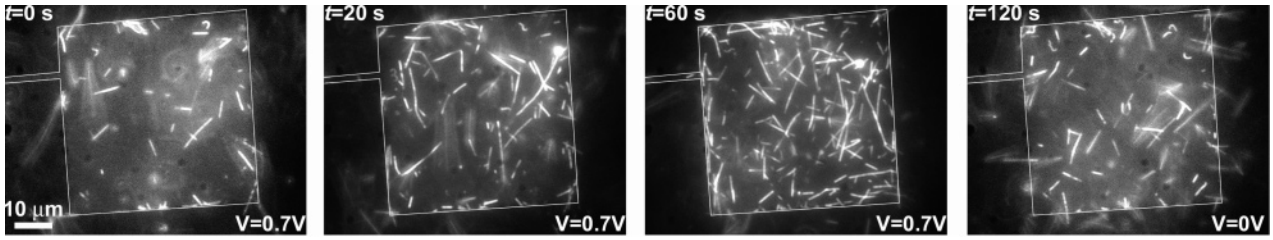


**Figure 2.** Docking of microtubules onto a Au microstructure upon application of a voltage of 0.7 V during 60 s. The number of microtubules inside the 50 × 50 $\mu$m$^2$ structure increases with time ($t$ = 0, $t$ = 20, $t$ = 60 s) during application of the voltage. After the voltage is switched off at $t$ = 60 s, the number of microtubules decreases again ($t$ = 120 s, 60 s after switching off the voltage). For clarity, the outline of the Au electrode is highlighted.

The image processing of the raw images consisted of a brightness-contrast-gamma correction and a convolution filter step to improve image quality (see Supporting Information). An automatic thresholding was then used to discriminate between microtubule particles and background. As a result, a binary version of each camera image was obtained with all microtubule pixels set to 1 and all background pixels set to 0. Finally, particles smaller than a critical size were removed. To determine the time evolution of the microtubule-covered area ($A$), this analysis was done for each camera image.

The result of this analysis is shown in Figure 3b, where we plot the microtubule-covered area during the event depicted in Figure 2. Upon application of the voltage at $t$ = 0 s, the surface coverage of microtubules starts to increase, from an initial value of ~$10^3$ pixels to ~20 × $10^3$ pixels at $t$ = 60 s. The microtubule density thus has increased more than an order of magnitude. After switching off the voltage ($t$ = 60 s), the surface coverage decreases again, in accordance with Figure 2, toward a value of ~$10^3$ pixels at $t$ = 125 s. From the time trace it is clear that the growth rate of microtubules on the surface levels off with increasing time. The decrease in coverage after switching off the voltage follows a similar time dependence. We found that both the growth and decay traces can be well fit with exponentials (red lines in Figure 3b).

In Figure 3a, we also plot the time evolution of the current density ($J_q$) during the same event. The values of $J_q$ were obtained by dividing the measured current by the area of the gold exposed to solution.[17] Upon application of the voltage, $J_q$ initially peaks and then a gradual decrease is observed. Within ~10 s the current density reaches an approximately constant value of about 35 A/m$^2$ (measured current ~200 nA).

As a further investigation, we show in Figure 3c and d similar data ($J_q$ and $A$) for a series of docking events measured in another experiment. In this measurement series, we applied a variety of pulse durations and amplitudes. The time evolutions of both $J_q$ and $A$ show a similar behavior as described above. We observe a correlation between the peak value of $A$ and the magnitude of $J_q$ in each event.

We attribute the transport of microtubules into the structures to migration as a result of the electrochemical current.[18] Upon application of a positive bias to the electrode, both $Fc(MeOH)_2$ and $\beta$ME are being oxidized at the electrode surface. Depletion of these redox species at the electrode surface leads to the development of an electric field in the solution, driving a migration current. A part of this migration current will be carried by negatively charged microtubules[6,13] in solution, resulting in the transport toward the electrode. The decrease of $J_q$ with time can be associated with the formation of a depletion region of electroactive species close to the electrode.[19] Both the data of the docking events upon application of a voltage, and the subsequent undocking data can be explained by considering the transport and the binding/unbinding of microtubules at the electrode surface.

We now develop a simple model to describe these data. We consider, on one hand, the transport of microtubules between the bulk and the surface, and on the other hand, the binding and unbinding dynamics of microtubules at the surface (Figure 4). We thus distinguish microtubules in three different states, viz., microtubules bound to kinesin molecules at the surface, free microtubules at the surface (but not bound to kinesin), and free microtubules in the bulk. Microtubules in the bulk (volume concentration [$M$]) can be transported toward the surface by both diffusion and migration. We denote the local volume concentration of microtubules in a small layer $dz$ above the surface as [$M_0$]. Microtubules within this distance $dz$ from the surface can bind to kinesin molecules with a rate, denoted $k'_b$, and start moving over the surface (surface concentration of bound microtubules [$MK$]). Bound microtubules can also detach from the surface with a rate $k_{off}$.

Considering first the transport of microtubules between the bulk and the surface, the rate of change in the total amount of microtubules (bound and free) at the surface is given as

$$\frac{\partial([MK] + dz\,[M_0])}{\partial t} = J_{\text{electric}} + J_{\text{diff}} \qquad (1)$$

where $J_{\text{electric}}$ and $J_{\text{diff}}$ are the migration and diffusion-driven fluxes of microtubules, respectively. We approximate the magnitude of $J_{\text{diff}}$ using the result for linear diffusion[19] as

$$J_{\text{diff}} = D_{\text{mt}}\frac{([M] - [M_0])}{h} = k_{\text{diff}}([M] - [M_0]) \qquad (2)$$

Here $k_{\text{diff}} = D_{\text{mt}}/h$, where $D_{\text{mt}}$ is the diffusion constant of a microtubule and $h$ is the length scale of the diffusion layer thickness. Upon application of a voltage to the electrode, an

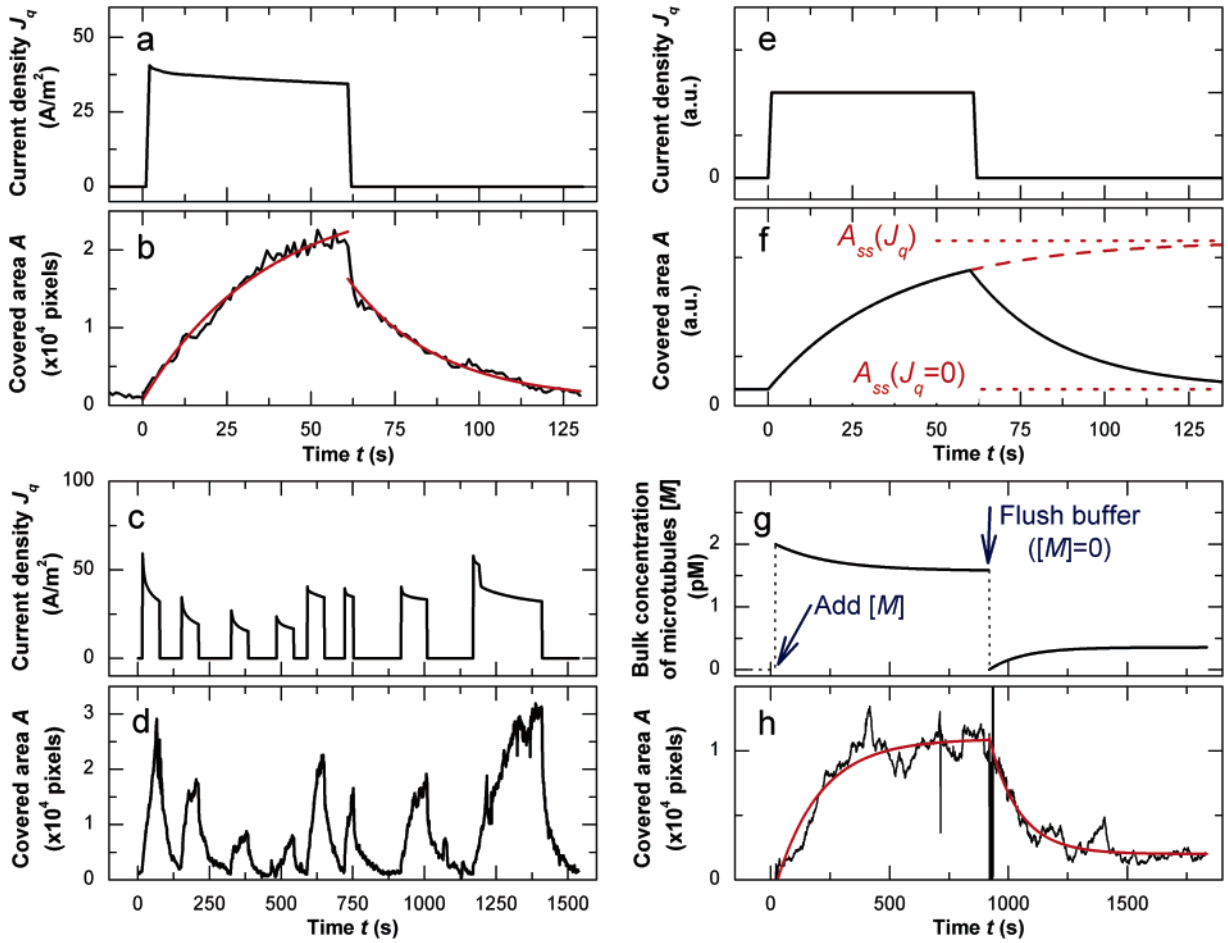


**Figure 3.** Time traces of the microtubule-covered area ($A$) and current density ($J_q$). (a,b) Measurement data of $A$ (b) and $J_q$ (a) corresponding to the event shown in Figure 2. The increase and decrease in area were fitted with exponentials (red lines, see text) with time constants $\tau$ equal to 37 and 27 s for the docking and undocking, respectively. (c,d) Series of docking and undocking events from a different experiment. A variety of voltage pulse durations (30 to 90 s) and amplitudes (0.55 to 0.75 V) was applied. The high noise in the $A(t)$ data present in the last event in Figure 3d is due to the passing of cluster of fluorescent material. (e,f) Results from an analytical model [eqs 6−8] describing the qualitative response in surface coverage (f) upon application of a block-shaped $J_q$ pulse of 60 s duration (e). Time constants were chosen in accordance with the time constants in (b) to facilitate a comparison. (g,h) Control experiment on a glass surface. Plotted is the measured change in surface coverage of microtubules on a glass slide (h) after changing the bulk microtubule concentration [$M$] (g). At $t$ = 0 s, microtubules are added and at $t$ = 900 s the flow cell was flushed with a motility solution without microtubules. The docking and undocking from the glass slide follow similar exponential time dependences (red lines). The plotted time dependence of [$M$] (g) is an estimate based on the fits in (h). All images contained 672 × 512 pixels.

electrochemical current starts to flow and microtubules migrate toward the electrode as a result of the electric field in the solution. The additional flux of microtubules is proportional to the bulk concentration and mobility of microtubules ($\mu_{mt}$) and the electric field in the bulk. The latter quantity equals $J_q/\sigma$ (with $\sigma$ the conductivity), yielding[18]

$$J_{electric} = \frac{\mu_{mt} J_q}{\sigma}[M] \qquad (3)$$

Finally, assuming equilibrium between [$MK$] and [$M_0$] at all times,[20] [$MK$] can be expressed as a fraction of the total amount of microtubules (bound and free) present at the surface:

$$[MK](t) = \frac{k_b}{k_b + dz\, k_{off}}([MK](t) + dz\,[M_0](t)) \qquad (4)$$

where $dz \cdot k'_b = k_b$. Combining eqs 1−4 yields for the rate of change in the concentration of microtubules bound to the surface:

$$\frac{\partial[MK]}{\partial t} = \frac{k_b}{k_b + dz\, k_{off}}\left(\left(k_{diff} + \frac{\mu_{mt} J_q}{\sigma}\right)[M] - \frac{k_{off} k_{diff}}{k_b}[MK]\right) \qquad (5)$$

To convert the surface concentration of microtubules [$MK$] into units of covered-area pixels ($A$), we use that $A = [MK]\text{-}N_A S a_0$. Here, $N_A$ is Avogadro's number, $S$ is the electrode area (in m$^2$) visible within the camera image, and $a_0$ is the average area of a microtubule in an image (in pixels). Using this transform and solving eq 5 (boundary condition $A_{t=0} = A_0$) under the assumption that the microtubule concentration in the bulk is constant,[21] we obtain for $A(t)$:

$$A(t) = A_{ss} + (A_0 - A_{ss}) \cdot e^{-t/\tau} \qquad (6)$$

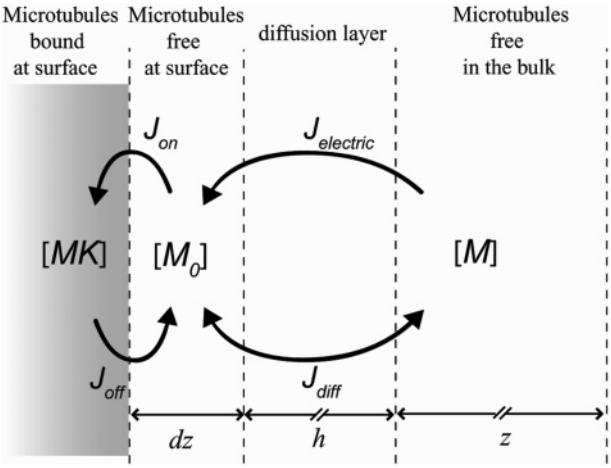


**Figure 4.** Schematic of the transport of microtubules between 3 different states. Microtubules can be transported between the bulk solution (volume concentration [$M$]) and the surface (local volume concentration [$M_0$]) via diffusion and via migration transport in the case of an electric field. Free microtubules close to the surface are in equilibrium with microtubules bound to kinesin molecules (surface concentration of kinesin-bound microtubules [$MK$]). Only microtubules that are within a distance $dz$ from the surface can interact with and bind to kinesin. The microtubule fluxes at the surface are denoted $J_{on}$ and $J_{off}$, for binding and unbinding, respectively. We denote the diffusion flux $J_{diff}$ (driven by a concentration gradient over a characteristic length $h$) and the migration flux $J_{electric}$. We denote the height of the flow cell as $z$.

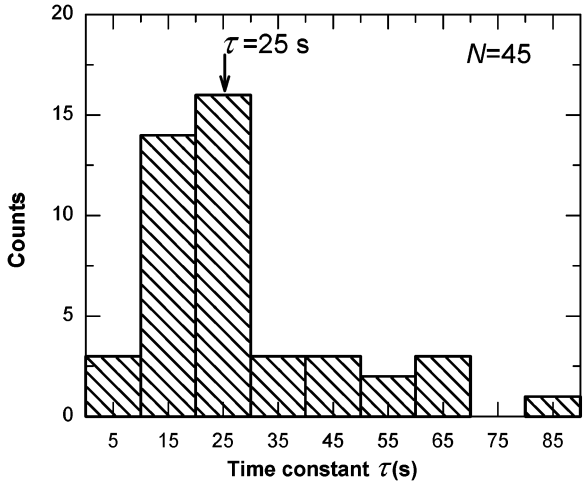


**Figure 5.** Histogram of time constants derived from fitting the undocking events. Events in both electrode structures (45 events) were used. The arrow indicates the median value. The inverse of the time constant equals $k_b/(k_{off}k_{diff}) = (\tau)^{-1} = 4 \times 10^{-2}$ s$^{-1}$.

where the time constant $\tau = (k_{off}k_{diff}/k_b)^{-1}$ under the assumption that $k_b \gg dzk_{off}$.[20] We will show later from the results that this assumption indeed holds. The steady-state coverage $A_{ss}$ is given by

$$A_{ss} = k_{on}(J_q)[M]\tau N_A S a_0 \quad (7)$$

where we defined an effective transport on-rate $k_{on}(J_q)$ as

$$k_{on}(J_q) = \left(k_{diff} + \frac{\mu_{mt}}{\sigma}J_q\right) \quad (8)$$

Figure 3 shows that eq 6 provides a good analytical description of the observed data. In Figure 3f we plot the time evolution of the covered area upon application of a block-shaped $J_q$ pulse of 60 s duration (Figure 3e). As a result of the $J_q$ there is an exponential growth in covered area from $A_0$ toward a steady-state coverage $A_{ss}$. The magnitude of $A_{ss}$ depends on $J_q$ according to eqs 7 and 8. Switching off $J_q$ leads to an exponential decay toward the initial $A_{ss}(J_q = 0)$.

We analyzed 45 docking and subsequent undocking events from 12 movies that were recorded in different experiments in two electrode sizes (50 and 100 $\mu$m lengths). First, all the undocking events were fitted with the model eq 6, with $A_0$, $A_{ss}$, and $\tau$ as free parameters. For each undocking event, we calculated the values of the binding affinity ratio $k_b/k_{off}$ and the diffusion transport rate $k_{diff}$ via eqs 7 and 8,[22] putting $J_q = 0$. The results of the fitted values for $\tau$, $k_b/k_{off}$, and $k_{diff}$ are displayed in Table 1. The distribution of time constants is given in Figure 5. A clear peak between 10 and 30 s is present in the data, with the median value of the distribution $\tau = 25 \pm 3$ s (standard error of the mean).

We compare the derived average value of $k_{diff}$, viz., $(5.3 \pm 0.8) \times 10^{-7}$ m/s (Table 1), with an estimate for $k_{diff}$ (eq 2). For the latter we use $D_{mt} = 4 \times 10^{-13}$ m$^2$/s, as calculated from the Einstein relation $D = k_BT/\gamma$. Here, $k_B$ is the Boltzmann constant, $T$ is the absolute temperature, and $\gamma$ is the drag coefficient. The value of $\gamma$ was analytically estimated to be $\gamma = 10^{-8}$ kg/s for a cylinder with the dimensions of a microtubule[23] (Supporting Information). Using this order-of-magnitude estimate for $D_{mt}$ we can calculate that, on the time scale of the experiments, the diffusion layer thickness $h$ is on the order of a few $\mu$m ($(h = (D_{mt}t)^{1/2})$. Thus we obtain a rough estimate for $k_{diff} = 10^{-7}$ m/s, which is in good agreement with the fitted value.

As a second step in the analysis, we used eq 6 to fit the data of the docking events in order to investigate the correlation between $A_{ss}$ and $J_q$. In the fitting procedure we

**Table 1.** Results Derived from Exponential Fits to Undocking Events

| structure | visible electrode area $S$ ($\mu$m$^2$) | time constant $\tau$ (s)[a] | diffusion rate $k_{diff}$ (m/s)[b] | binding affinity $k_b/k_{off}$ (m)[b] |
|---|---|---|---|---|
| small electrode ($N = 16$) | 2500 | $24 \pm 2$ | $(6.2 \pm 1.4) \times 10^{-7}$ | $(9.8 \pm 1.3) \times 10^{-6}$ |
| large electrode ($N$=29) | 4880 | $25 \pm 4$ | $(4.8 \pm 1.0) \times 10^{-7}$ | $(9.1 \pm 1.2) \times 10^{-6}$ |
| all events ($N = 45$) | not applicable | $25 \pm 3$ | $(5.3 \pm 0.8) \times 10^{-7}$ | $(9.3 \pm 0.9) \times 10^{-6}$ |

[a] Median value of the distribution ± standard error of the mean. [b] Average ± standard error of the mean.

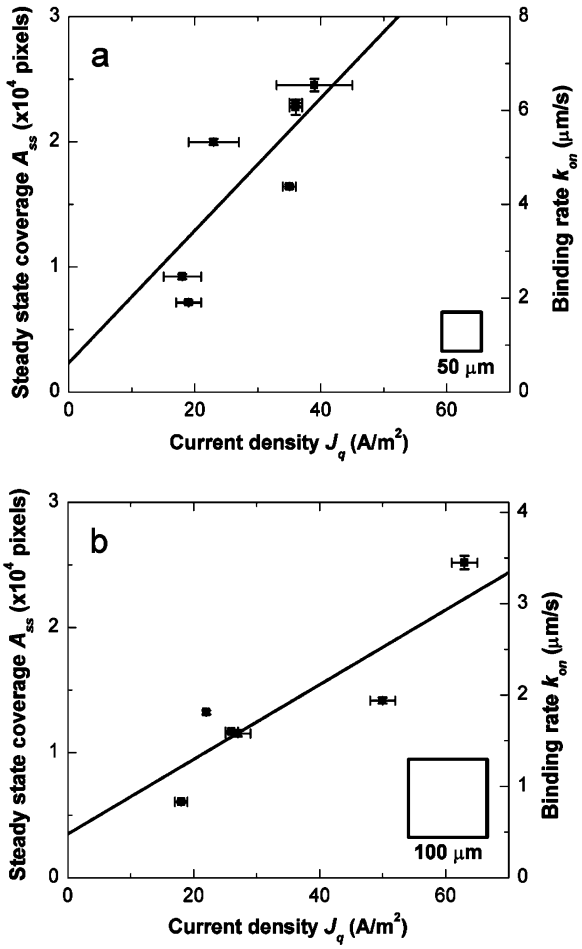


**Figure 6.** Steady-state microtubule coverage as a function of current density at the electrode. Lines are least-squares fits through the data with the *y*-axis intercept fixed at the $k_{diff}$ values for each electrode size (Table 1). (a) Data recorded in a (50 $\mu$m)$^2$-sized electrode; data points corresponding to events shown in Figure 3c and d. The fit has a slope $\partial k_{on}/\partial J_q = 1.4 \times 10^{-7}$ m$^3$/As ($\partial A_{ss}/\partial J_q = 5.6 \times 10^2$ pixels m$^2$/A). (b) Data for a movie recorded in a (100 $\mu$m)$^2$-sized electrode. Slope $\partial k_{on}/\partial J_q = 4.1 \times 10^{-8}$ m$^3$/As from the fit ($\partial A_{ss}/\partial J_q = 2.9 \times 10^2$ pixels m$^2$/A).

fixed the time constant to be $\tau = 25$ s, as found from the undocking events (Table 1), and we fitted the $A_{ss}$ values. We obtained $A_{ss}$ for each docking event and we can evaluate this versus the measured current density $J_q$.

Figure 6 shows fitted $A_{ss}$ data versus measured $J_q$ for two different electrode sizes. Each plot shows a series of docking events for a typical experiment. In agreement with eqs 7 and 8, there is a clear increase in the binding rate of microtubules with increasing current density. Although the scatter in the data points is considerable, we expect from the model that the increase is linear. The straight lines in Figure 6 are least-squares fits to the $k_{on}(J_q)$ data points, where the intercept with the *y*-axis ($k_{on}(J_q = 0) = k_{diff}$, eq 8) was set by the values given in Table 1. For the slopes we find values of $\partial k_{on}/\partial J_q = 1.4 \times 10^{-7}$ m$^3$ A$^{-1}$ s$^{-1}$ and $4.1 \times 10^{-8}$ m$^3$ A$^{-1}$ s$^{-1}$ for Figure 6a and b, respectively. The predicted value of the slope, according to eq 8, is determined by the microtubule mobility and the conductivity, viz.,[22] $\partial k_{on}/\partial J_q = \mu_{mt}/\sigma \sim 4 \times 10^{-8}$ m$^3$ A$^{-1}$ s$^{-1}$. This is of the same order of magnitude as the values found from the fits (Figure 6). We attribute the difference in the slopes between the two plots mainly to the uncertainty in the $J_q$ values (we cannot compare the $J_q$ scales due to the different sizes of the electrodes[17]). We emphasize that the value that we find for $\mu_{mt}/\sigma$ is an order of magnitude estimate, which we find in reasonable agreement with the analytical value.

We confirm the validity of the equilibrium model for docking and undocking of microtubules to a surface with a control experiment on a glass surface (Figure 3h). Here, we measured the time evolution of microtubules binding to a kinesin-coated glass slide in a flow cell consisting of two glass cover slides separated by 100 $\mu$m thick spacers. At $t = 20$ s we flushed the flow cell with motility solution containing 2 pM microtubules (Figure 3g). As predicted from the model, the microtubule population on glass grows exponentially toward an equilibrium value. Then, at $t \sim 920$ s the flow cell was flushed with a motility solution without microtubules, effectively setting $[M] = 0$ at that time (second arrow in Figure 3g). As a result, the population of microtubules bound to the glass flow cell decreases exponentially toward its new equilibrium value. We can compare the rate constants for microtubule docking onto our gold microstructures with the docking observed on a macroscopic glass slide. In the case of a glass flow cell the value of $[M]$ cannot be taken constant during the experiment.[21] This results in a slight modification in the expressions for $\tau$ and $A_{ss}$, but the qualitative behavior for the surface coverage is similar. From the fits in Figure 3h we calculate (Supporting Information) a binding affinity of microtubules on a glass surface of $k_b/k_{off} \sim 2 \times 10^{-5}$ m. This is slightly higher than the value $0.9 \times 10^{-5}$ m found for the gold surfaces in our structures, in line with the observation that the microtubule density on glass (Figure 3h, $A_{ss} \sim 10^4$ pixels in a $61 \times 80$ $\mu$m$^2$ camera image) is usually slightly higher than on gold surfaces without applied voltage (Figure 3d, $A_{ss}(J_q = 0) \sim 10^3$ pixels in a $50 \times 50$ $\mu$m$^2$ electrode area).

In conclusion, we have observed the electrostatic docking of microtubule shuttles into microfabricated structures after application of a voltage. The microtubule coverage on the gold surface exponentially approaches a steady-state equilibrium value ($A_{ss}$). The value of $A_{ss}$ is found to be linearly dependent on the current density flowing through the electrode. Switching off the applied voltage leads to the partial undocking of microtubules, again displaying an exponential dependence. We provided a simple kinetic model for the equilibrium between microtubules in solution and microtubules bound to kinesin at the surface. From this model, we estimated the binding affinity of microtubules for a gold surface to be $k_b/k_{off} = 0.9 \times 10^{-5}$ m, which is lower than for a glass surface ($k_b/k_{off} = 2 \times 10^{-5}$ m). From the data we also derived that the diffusion-driven transport rate $k_{diff}$ of microtubules into square gold electrodes was $k_{diff} = (5.3 \pm 0.8) \times 10^{-7}$ m/s. We achieved a $J_q$-dependent increase of the microtubule-transport rate (up to a 10-fold increase compared to $k_{diff}$) by applying a voltage to the gold surface. We attribute this effect to migration of microtubules. We have shown that the same model also describes the binding

and unbinding to a glass surface. The use of localized electric fields in nanofabricated structures and the better understanding of the binding dynamics of microtubule shuttles to a surface will be useful for the future exploitation of biomolecular motors in a nanotransport system.

**Acknowledgment.** We thank H. A. Heering, and B. M. Quinn for discussions about the electrochemical aspects of this work and D. Korbee for wire bonding of the samples. We acknowledge R. M. M. Smeets for involvement in the preliminary stages of the nanofabrication work. S. D. acknowledges support from the BMBF (grant 03N8712).

**Supporting Information Available:** Movie of electrical docking of microtubules and further information with pictures of the image processing steps. Additional mathematical derivations and numerical estimates. This material is available free of charge via the Internet at http://pubs.acs.org.

## References

(1) Hess, H.; Vogel, V. *Rev. Molec. Biotechnol.* **2001**, *82*(1), 67−85.
(2) Hess, H.; Bachand, G. D.; Vogel, V. *Chem.−Eur. J.* **2004**, *10*(9), 2110−2116.
(3) Diez, S.; Reuther, C.; Dinu, C.; Seidel, R.; Mertig, M.; Pompe, W.; Howard, J. *Nano Lett.* **2003**, *3*(9), 1251−1254.
(4) Hess, H.; Clemmens, J.; Qin, D.; Howard, J.; Vogel, V. *Nano Lett.* **2001**, *1*(5), 235−239.
(5) Bachand, G. D.; Rivera, S. B.; Boal, A. K.; Gaudioso, J.; Liu, J.; Bunker, B. C. *Nano Lett.* **2004**, *4*(5), 817−821.
(6) Jia, L. L.; Moorjani, S. G.; Jackson, T. N.; Hancock, W. O. *Biomed. Microdevices* **2004**, *6*(1), 67−74.
(7) Moorjani, S. G.; Jia, L.; Jackson, T. N.; Hancock, W. O. *Nano Lett.* **2003**, *3*(5), 633−637.
(8) Hiratsuka, Y.; Tada, T.; Oiwa, K.; Kanayama, T.; Uyeda, T. Q. P. *Biophys. J.* **2001**, *81*(3), 1555−1561.
(9) Clemmens, J.; Hess, H.; Lipscomb, R.; Hanein, Y.; Bohringer, K. F.; Matzke, C. M.; Bachand, G. D.; Bunker, B. C.; Vogel, V. *Langmuir* **2003**, *19*(26), 10967−10974.
(10) Bunk, R.; Klinth, J.; Rosengren, J.; Nicholls, I.; Tagerud, S.; Omling, P.; Mansson, A.; Montelius, L. *Microelectron. Eng.* **2003**, *67-8*, 899−904.
(11) Nicolau, D. V.; Suzuki, H.; Mashiko, S.; Taguchi, T.; Yoshikawa, S. *Biophys. J.* **1999**, *77*(2), 1126−1134.
(12) Suzuki, H.; Yamada, A.; Oiwa, K.; Nakayama, H.; Mashiko, S. *Biophys. J.* **1997**, *72*(5), 1997−2001.
(13) Stracke, R.; Bohm, K. J.; Wollweber, L.; Tuszynski, J. A.; Unger, E. *Biochem. Biophys. Res. Commun.* **2002**, *293*(1), 602−609.
(14) Riveline, D.; Ott, A.; Julicher, F.; Winkelmann, D. A.; Cardoso, O.; Lacapere, J. J.; Magnusdottir, S.; Viovy, J. L.; Gorre-Talini, L.; Prost, J. *Eur. Biophys. J.* **1998**, *27*(4), 403−408.
(15) Asokan, S. B.; Jawerth, L.; Carroll, R. L.; Cheney, R. E.; Washburn, S.; Superfine, R. *Nano Lett.* **2003**, *3*(4), 431−437.
(16) Microtubules were polymerized from 10 $\mu$L of bovine brain tubulin (4 mg/mL, 1 rhodamine labeled unit, 3 unlabeled units, Cytoskeleton, Denver, CO) in the presence of 4 mM $MgCl_2$, 1 mM GTP, and 5% DMSO in BRB80 buffer (37 °C for 60 min). Then the microtubules were stabilized and 100× diluted in BRB80 containing 10 $\mu$M Taxol (BRB80T). The final tubulin concentration would then be ∼32 nM. For the experiments in the 100 $\mu$m sized electrode, the 10 $\mu$L of polymerized microtubules were stabilized and diluted 40× in BRB80T. To remove the unpolymerized tubulin, the 400 $\mu$L was centrifuged at 178.000 g in a Beckman airfuge for 5 min and the pellet was resuspended in 1000 $\mu$L of BRB80T, yielding again a tubulin concentration of ∼32 nM. In all experiments, we shortened the microtubules by shearing them in a 30 g needle.
(17) The connection leads had ∼1500 × 2 $\mu m^2$ area ($A_{lead}$) exposed to the solution, which is significant compared to the areas of the square structures ($A_{square}$). To calculate the current density we therefore divided the measured current by the total exposed gold area ($A_{lead} + A_{square}$). In general the diffusion-limited current density is dependent on the geometry of the electrode.[19] The observed $J_q$, therefore, should be a weighted average of the $J_q$ values for a square and rectangular microelectrode, and $J_q$ as calculated in our procedure does not necessarily equal the exact current density at the square electrode. Also, because the ratio $A_{lead}/A_{square}$ is different for the 50 and 100 $\mu$m-sized structures, the calculated $J_q$ values can not, strictly speaking, be directly compared between both electrode sizes.
(18) Quinn, B. M.; van't Hof, P.; Lemay, S. G. *J. Am. Chem. Soc.* **2004**, *126*(27), 8360−8361.
(19) Bard, A. J.; Faulkner, L. R. *Electrochemical methods*, 2nd ed.; John Wiley & Sons: New York, 2001.
(20) The assumption of assuming equilibrium between [*MK*] and [$M_0$] is equivalent to assuming that ($k_b + dz\ k_{off}$) ≫ $k_{diff}$. From the experiments we derive that $k_b \gg dz\ k_{off}$ (upon adopting a reasonable value for $dz = 10^{-8}$ m), so the surface-equilibrium assumption simplifies to assuming $k_b \gg k_{diff}$. Although the validity of this statement cannot be directly confirmed from the data (as we have no way to extract the value of $k_b$ from the data), we *can* show that the less strict condition $k_b \geq k_{diff}$ does hold. In the most pessimistic case $k_b \approx k_{diff}$, the fitted values for $k_{diff}$ and $\mu_{mt}/\sigma$ then represent lower bounds, while the presented value of $k_b/k_{off}$ is still exact. We also solved the model under the opposite assumption ($k_b \ll k_{diff}$) and made fits to the data. This yielded values for $k_b$ and $k_{diff}$ that were the same order of magnitude ($k_b \approx k_{diff}$), thereby invalidating the assumption that $k_b \ll k_{diff}$ and ruling out this possibility.
(21) The approximation that [*M*] is a constant is valid as long as the amount of microtubules docking into a structure is insignificant compared to the total number of microtubules in solution. In the electrically controlled docking experiments, this assumption holds well since the electrode area is small. Viz., the total number of microtubules inside the flow cell volume (∼5 $\mu$L) is estimated as ∼3 × $10^6$, while the number of microtubules attracted inside an electrode structure is much smaller, ∼$10^2$−$10^3$. For the control experiment in a glass flow cell (Figure 3h), however, [*M*] is changed significantly during the experiment, since microtubules dock over the entire flow cell area. From Figure 3h we estimate ∼$10^6$ microtubules moving on the glass, a significant part of the number of microtubules in solution (Figure 3g). As a result, the expressions for $\tau$ and $A_{ss}$ are slightly modified in this control experiment. (See Supporting Information for derivations).
(22) We used the following values for the different variables: $\mu_{mt} = 3 \times 10^{-8}$ $m^2$/Vs (from ref 13), $a_0 = 100$ pixels/microtubule (determined from camera images), and $\sigma = 0.7$ A/Vm (measured with a conductivity meter). The microtubule concentration in all experiments was estimated to be [*M*]∼$10^{-12}$ M. This value was calculated assuming complete polymerization from the tubulin concentration of ∼32 nM, an average microtubule length of 5 $\mu$m, and each microtubule containing ∼$10^4$ tubulin dimers.
(23) Hunt, A. J.; Gittes, F.; Howard, J. *Biophys. J.* **1994**, *67*(2), 766−781.

NL048291N